Journal of Advanced Research 9 (2018) 51–61

Contents lists available at ScienceDirect

Journal of Advanced Research

journal homepage: www.elsevier.com/locate/jare

Highly functionalized piperidines: Free radical scavenging, anticancer activity, DNA interaction and correlation with biological activity

Suvankar Das [a], Cristiane J. da Silva [b], Marina de M. Silva [c], Maria Dayanne de A. Dantas [c], Ângelo de Fátima [d,*], Ana Lúcia T. Góis Ruiz [e], Cleiton M. da Silva [d], João Ernesto de Carvalho [e], Josué C.C. Santos [c], Isis M. Figueiredo [c], Edeildo F. da Silva-Júnior [c,f], Thiago M. de Aquino [c,f], João X. de Araújo-Júnior [c,f], Goutam Brahmachari [a,*], Luzia Valentina Modolo [b]

[a] Department of Chemistry, Visva-Bharati (a Central University), Santiniketan 731 235, West Bengal, India
[b] Department of Botany, Universidade Federal de Minas Gerais, Belo Horizonte, MG, Brazil
[c] Institute of Chemistry and Biotechnology, Universidade Federal de Alagoas, Maceió, AL, Brazil
[d] Department of Chemistry, Universidade Federal de Minas Gerais, Belo Horizonte, MG, Brazil
[e] Chemical, Biological and Agricultural Pluridisciplinary Research Center, Universidade Estadual de Campinas, Paulínia, SP, Brazil
[f] Laboratory of Medicinal Chemistry, Nursing and Pharmacy School, Universidade Federal de Alagoas, Maceió, AL, Brazil

GRAPHICAL ABSTRACT

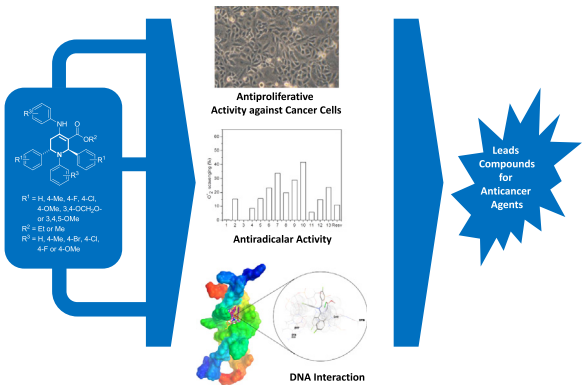

ARTICLE INFO

Article history:
Received 12 August 2017
Revised 29 October 2017
Accepted 30 October 2017
Available online 31 October 2017

Keywords:
Piperidine derivatives
Free radical scavenging

ABSTRACT

Twenty-five piperidines were studied as potential radical scavengers and antitumor agents. Quantitative interaction of compounds with ctDNA using spectroscopic techniques was also evaluated. Our results demonstrate that the evaluated piperidines possesses different abilities to scavenge the radical 2,2-diphenyl-1-picrylhydrazyl (DPPH) and the anion radical superoxide ($\cdot O_2^-$). The piperidine **19** was the most potent radical DPPH scavenger, while the most effective to $\cdot O_2^-$ scavenger was piperidine **10**. In general, U251, MCF7, NCI/ADR-RES, NCI-H460 and HT29 cells were least sensitive to the tested compounds and all compounds were considerably more toxic to the studied cancer cell lines than to the normal cell line HaCaT. The binding mode of the compounds and ctDNA was preferably via intercalation.

Peer review under responsibility of Cairo University.
* Corresponding authors.
E-mail addresses: adefatima@qui.ufmg.br (Â. de Fátima), goutam.brahmachari@visva-bharati.ac.in, brahmg2001@yahoo.co.in (G. Brahmachari).

https://doi.org/10.1016/j.jare.2017.10.010
2090-1232/

Anticancer activity
DNA interaction

In addition, these results were confirmed based on theoretical studies. Finally, a linear and exponential correlation between interaction constant (K_b) and GI_{50} for several human cancer cell was observed.

Introduction

Nitrogen-containing heterocyclic compounds are widely found in natural products and pharmaceuticals [1]. Many of them play essential functions in the human organism and present significant biological properties [2].

Piperidines and their derivatives comprise a major class of *N*-heterocycles of biological interest. Compounds bearing the piperidine moiety exhibit a broad range of biological properties, including anti-hypertensive [3], antibacterial [4], antimalarial [5], anti-inflammatory [6], analgesic [7,8], antioxidant [9], and antiproliferative activities [10].

Currently, several compounds containing the piperidine nucleus are employed in the current clinical as drug for treating diseases. Donepezil (Fig. 1), a potent, specific, non-competitive and reversible inhibitor of acetylcholinesterase is prescribed to treat patients with Alzheimer's disease [11]. Pipamperone (Fig. 1), other 1,4-substituted piperidine derivative, is indicated for patients with schizophrenia [12]. Vinblastine (Fig. 1), a naturally occurring alkaloid derived from *Catharanthus roseus*, is used as anticancer agent for a wide variety of cancers including non-small cell lung cancer, breast cancer, bladder cancer, lymphomas, and leukemia [13].

Due to their pronounced biological properties, various synthetic methods have been developed for the synthesis of piperidine derivatives [14]. Recently, we described the synthesis of highly functionalized piperidines from multicomponent reactions catalyzed by bismuth nitrate [14]. Here, we report the evaluation of the activity of the previously synthesized compounds as scavengers of reactive nitrogen and oxygen species (RNS and ROS, respectively) and cancer cell proliferation inhibitors. Additionally, the interactions of selected compounds with the DNA were evaluated, since several pathologies have DNA as the main biological target.

Experimental

Scavenging of reactive nitrogen species

The ability of piperidine derivatives **1–25** to scavenge 2,2-diphenyl-1-picrylhydrazyl (DPPH; Sigma, MO, USA) radical, a reactive nitrogen species (RNS), was determined according to Gülçin [15], with modifications. Each compound-test (64 μM) in an ethanolic medium containing DMSO 0.64 % (Sigma, MO, USA) was incubated with DPPH (100 μM). The systems were maintained under stirring and absence of light for 30 min and the absorbance recorded at 517 nm. The experiments were performed in quadruplicate and resveratrol was used as positive control.

Scavenging of reactive oxygen species

The capacity of piperidine derivatives to scavenge superoxide anions ($.O_2^-$), was determined according to da Silva et al. [16], with modifications. Test-compounds at a concentration of 80 μM (0.8% DMSO/ethanol), were incubated in the presence of 60% (v/v) ethanol, 100 μM EDTA (Sigma, MO, USA), 13.3 mM L-methionine (Sigma, MO, USA), 200 μM nitroblue tetrazolium (NBT; Sigma, MO, USA) and 40 μM riboflavin (Sigma, MO, USA). Reaction mixtures were incubated for 10 min at 25 °C in the presence of fluorescent light to induce $^{\cdot}O_2^-$ formation. Controls consisted of

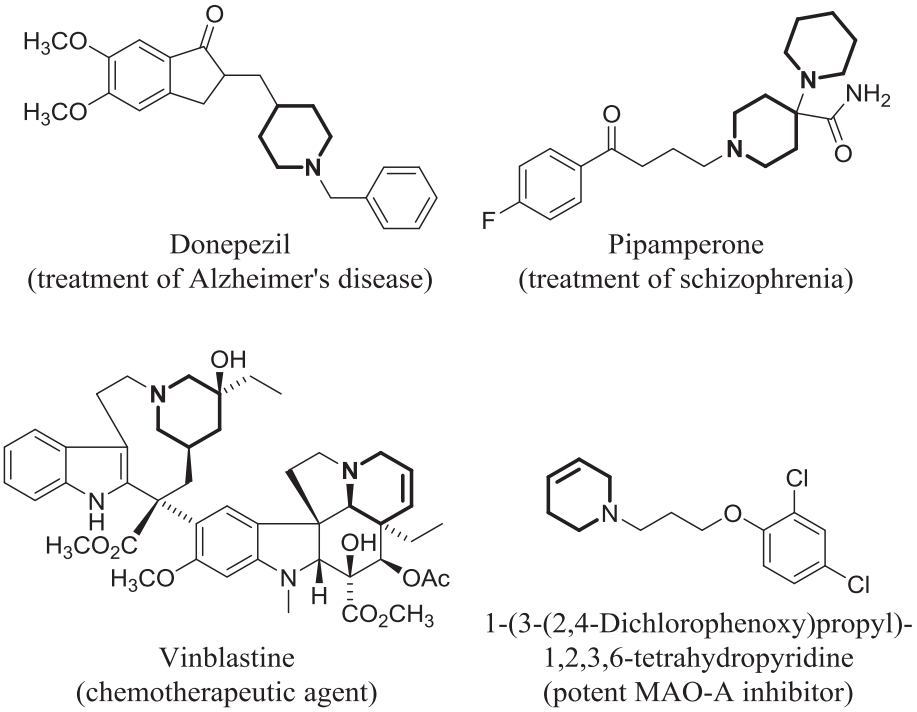

Fig. 1. Examples of piperidine derivatives with remarkable biological activities.

reaction mixtures kept at 25 °C for 10 min in absence of light. The percentage of $^{\cdot}O_2^-$ scavenged by each compound-test was determined through spectrophotometric analysis at 575 nm. The experiments were performed in quadruplicate and resveratrol was used as positive control.

Antiproliferative assay

Human tumor cell lines U251 (glioma), MCF7 (breast), NCI/ADR-RES (ovarian expressing the resistance phenotype for adryamycin), 786-0 (kidney), NCI-H460 (lung, non-small cells), PC-3 (prostate), HT29 (colon), and normal cell line HaCaT were kindly provided by Frederick Cancer Research & Development Center - National Cancer Institute - Frederick, MA, USA. Stock cultures were grown in RPMI 1640 (GIBCO BRL, Life Technologies) supplemented with 5% fetal bovine serum, penicillin (final concentration of 1 $mg{\cdot}mL^{-1}$) and streptomycin (final concentration of 200 $U{\cdot}mL^{-1}$) [17–19]. Cells in 96-well plates (100 μL cells/well) were exposed to piperidines synthesized (0.25–250 $\mu g{\cdot}mL^{-1}$) for 48 h at 37 °C and 5% CO_2. The cells were then fixed with 50% trichloroacetic acid and submitted to sulforhodamine B assay for cell proliferation quantitation at 540 nm [20]. The compound concentration that inhibits cell growth by 50% (GI_{50}) was determined through non-linear regression analysis using the software ORIGIN 7.5 (OriginLab Corporation). Doxorubicin was used as a reference drug. Results presented are from two independent experiments, each done in triplicate.

DNA interaction

Apparatus

Molecular fluorescence measurements were performed on Shimadzu spectrofluorimeter (model 5301PC, Japan) equipped with a xenon lamp (150 W) and using quartz cuvettes of 10 mm optical path. The molecular absorption measurements were performed in a scanning spectrophotometer Micronal (AJX-6100PC model, Brazil) with double-beam equipped with quartz cuvettes of 10 mm optical path.

Chemicals and solutions

All reagents used were of high analytical purity. The stock solution of *Calf thymus* DNA (ctDNA; Sigma, MO, USA) was prepared in Tris-HCl buffer (10 mM, pH = 7.4 ± 0.10; Sigma, MO, USA) with 0.1 M of NaCl for the ionic strength adjustment. To evaluate nucleic acid purity, the absorbance at 260 and 280 nm was measured, and when A_{260}/A_{280} = 1.8–1.9 indicates that the macromolecule is free from protein contamination. In addition, to calculate the DNA concentration the A_{260} was used, with a molar extinction coefficient of 6600 L mol^{-1} [21].

The piperidine derivatives were initially solubilized in DMSO (Sigma, MO, USA) and then, diluted in buffer solution. In the fluorimetric titration studies the concentration of each compound was maintained fixed at 10 μM, and increments concentration of DNA ranging from 10 to 200 μM were added. In the assays to evaluate the preferential binding mode with the ctDNA, it was used a stock solution of potassium iodide at 0.2 M, and a solution of ethidium bromide at 0.5 mM, using as instrumental parameters λ_{ex} = 525 nm/λ_{em} = 590 nm.

Dynamics simulation

The coordinates for building the molecular model were extracted from the X-ray crystal structure of the DNA dodecamer d(CGCGAATTCGCG) (PDB ID: 1BNA), available at doi 10.2210/pdb1bna/pdb. All molecular dynamic proceeds were performed in agreement with Silva et al. [22].

Molecular docking

Computational methodologies, such as molecular docking, have been employed to providing new scaffolds with high potency and good tolerance [23]. After molecular dynamic completion, the optimized ct-DNA structure with the lowest RMSD value was used in this study [24]. Molecular docking was performed in tentative to observe some aspects in the formation of complexes, such as nitrogenous bases involvement, binding mode, type of interaction, and best conformation. All methods were performed as described by Silva et al. [24].

Results and discussion

Scavenging of free radical species

It is well documented that free radicals, which are generated in many bioorganic redox processes, are able to oxidize nucleic acids, proteins, lipids and/or DNA and can then initiate degenerative diseases, including cancer, arthritis, hemorrhagic shock, age-related degenerative brain diseases [25–27]. In 2012, Prashanth et al. [27] reported that piperamides bearing piperidine or piperazine groups possesses substantial scavenging properties with potencies ranging from 8.3 ± 0.02 to 36.9 ± 0.17 $\mu g{\cdot}mL^{-1}$ (against DPPH radical) and 12.8 ± 0.08 to 55.3 ± 0.17 $\mu g{\cdot}mL^{-1}$ (against $^{\cdot}O_2^-$). Taking these information in account, the previously synthesized piperidine derivatives **1**–**25** (Fig. 2) [14] were then evaluated for their ability to capture reactive nitrogen species (RNS) and reactive oxygen species (ROS).

The radical 2,2-diphenyl-1-picrylhydrazyl (DPPH) was used as source of RNS and the anion radical superoxide ($^{\cdot}O_2^-$) was used as source of ROS. Resveratrol (Resv), a known antioxidant derived from plants, was used as a positive control. The percentages of DPPH and $^{\cdot}O_2^-$ scavenged by piperidine derivatives are shown, respectively, in Figs. 3 and 4.

In general, the tested compounds were more effective in scavenging reactive nitrogen species. The capture percentages ranged from 18 to 44%, *versus* 62% observed for resveratrol. Among the twenty-five compounds evaluated fourteen showed captures higher than 25 % at a concentration of 64 μM. Compound **9** was the most active, with 44% capture in concentration evaluated (Fig. 3).

In reactive oxygen species ($^{\cdot}O_2^-$) tests, five of the compounds, at a concentration of 80 μM, evaluated showed capture percentages higher than 25%, while resveratrol captured only 11% (Fig. 4). Compound **10** proved to be the most active, capturing 42% of the radical species. Piperidine derivatives **7**, **9**, **21**, and **22** were also promising scavengers, since they removed 34, 29, 33, and 36% of ROS present in the reaction medium, respectively. To our best acknowledgment, this is the first study on the potential of piperidine derivatives to scavenge ROS and RNS.

Antiproliferative activities

Since the piperidine nucleus is present in many biologically active compounds, we investigated the effect of compounds **1**–**25** on proliferation of eight cancer cells lines from various histological origins, including U251 (glioma), MCF7 (breast), NCI/ADR-RES (ovarian expressing the resistance phenotype for adryamycin), 786-0 (kidney), NCI-H460 (lung, non-small cells), PC-3 (prostate) and HT29 (colon). The antiproliferative effect of these piperidines derivatives was also evaluated against HaCaT (human keratinocyte) in order to verify their toxicity to normal cells. Cell proliferation was determined by spectrophotometric measurements using sulforhodamine B as a protein-binding dye and doxorubicin (DOX; 0.025–25 $\mu g{\cdot}mL^{-1}$) as a reference drug. The concentrations

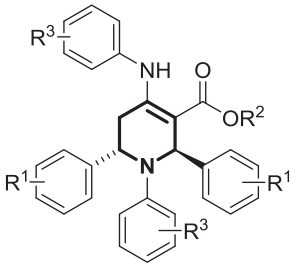

1. R^1 = H, R^2 = Et, R^3 = H
2. R^1 = H, R^2 = Me, R^3 = H
3. R^1 = 4-Me, R^2 = Me, R^3 = H
4. R^1 = 4-Me, R^2 = Et, R^3 = H
5. R^1 = 4-Me, R^2 = Me, R^3 = 4-Me
6. R^1 = 4-Me, R^2 = Me, R^3 = 4-Br
7. R^1 = 4-Me, R^2 = Me, R^3 = 4-Cl
8. R^1 = 4-Me, R^2 = Me, R^3 = 4-OMe
9. R^1 = 4-Me, R^2 = Et, R^3 = 4-OMe
10. R^1 = H, R^2 = Et, R^3 = 4-OMe
11. R^1 = H, R^2 = Et, R^3 = 4-Cl
12. R^1 = H, R^2 = Et, R^3 = 4-Me
13. R^1 = H, R^2 = Me, R^3 = 4-F
14. R^1 = 4-Cl, R^2 = Et, R^3 = 4-F
15. R^1 = 4-F, R^2 = Et, R^3 = H
16. R^1 = 4-F, R^2 = Me, R^3 = 4-F
17. R^1 = 4-F, R^2 = Me, R^3 = 4-Cl
18. R^1 = H, R^2 = *t*-Bu, R^3 = H
19. R^1 = 4-Cl, R^2 = Me, R^3 = H
20. R^1 = 4-Cl, R^2 = Et, R^3 = 4-Me
21. R^1 = 4-Cl, R^2 = Me, R^3 = 4-Br
22. R^1 = 4-OMe, R^2 = Me, R^3 = 4-Br
23. R^1 = 4-OMe, R^2 = Et, R^3 = 4-Cl
24. R^1 = 3,4-OCH_2O-, R^2 = Me, R^3 = H
25. R^1 = 3,4,5-OMe, R^2 = Me, R^3 = H

Fig. 2. Structures of previously synthesized piperidine derivatives.

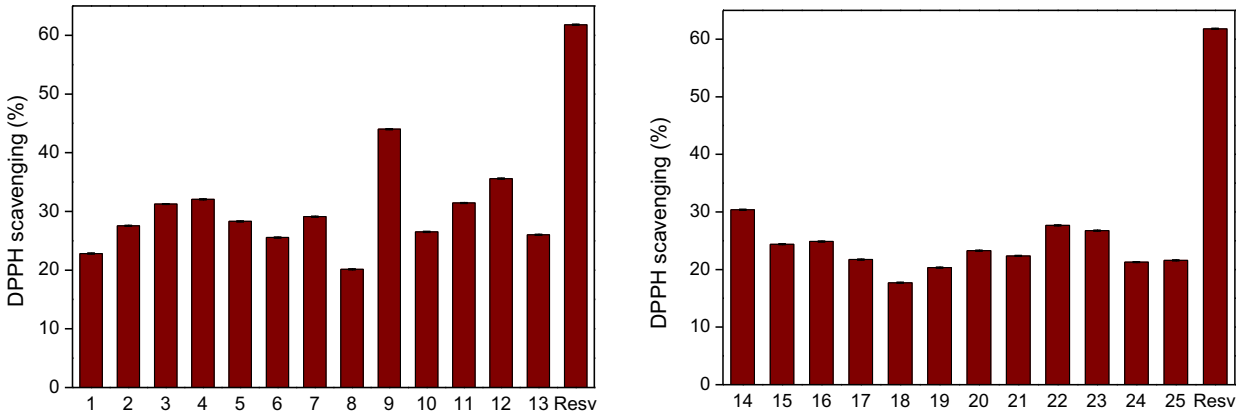

Fig. 3. Percentages of reactive nitrogen species scavenged by piperidine derivatives **1**–**25**. The reaction medium consisted of compound-test (64 μM) and DPPH radical (100 μM). Resveratrol (Resv) was employed as a positive control. Data are the means ± SD of three independent experiments, each done in triplicate. SD deviations were lower than 0.015%.

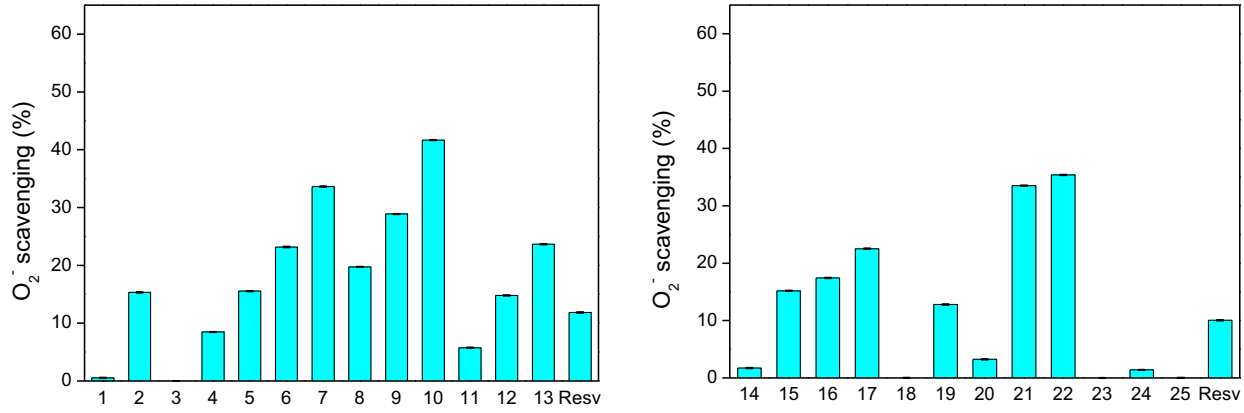

Fig. 4. Percentages of reactive oxygen species scavenged by piperidine derivatives **1**–**25**. The production of $^{\cdot}O_2^-$ was induced as described in experimental section. Each compound-test was employed at a concentration of 80 μM. Resveratrol (Resv) was employed as a positive control. Data are the means ± SD of three independent experiments, each done in triplicate. SD deviations were lower than 0.05%.

of compounds that elicited the inhibition of cell growth by 50% (GI_{50}) and their selective indexes (SI) are summarized in Table 1. The SI is herein defined as the ratio of the GI_{50} of pure compound in a normal cell line (*i.e.* HaCat cell line) to the GI_{50} of the same pure compound in a cancer cell line.

PC-3 was the most sensitive cancer cell line. Among all compounds evaluated, piperidine derivatives **1**, **2**, **3**, **7**, **10**, **16**, **21**, **22**, and **25** were the most active against this line, with GI_{50} values ≤ 25 μg·mL^{-1}, highlighting the compounds **1** and **25**, which exhibited GI_{50} values of 6.3 and 6.4 μg mL^{-1}, respectively (Table 1). As the value of SI indicates a differential activity of a compound-test, it is noteworthy to mention that compounds **1** and **25** also presented the highest SI values (≥39.0; Table 1) for PC-3 cancer cell line. These SI values are, at least, 10-fold higher than the value expected for a high selective candidate compound in *in vitro* preclinical trials [28,29]. Besides these interesting results, compounds

Table 1
Cytotoxicity activity (GI_{50}[a] values, in $\mu g \cdot mL^{-1}$) and selective index (SI[b]; given in parentheses) of functionalized piperidines and doxorubicin (DOX)[c] against cancer cell lines.

Compound	Cell line[d]							
	U251	MCF7	NCI/ADR-RES	786–0	NCI-H460	PC-3	HT29	HaCaT
1	>250	>250	>250	113.9 (>2.2)	>250	6.3 (>39.7)	>250	>250
2	>250	>250	>250	20.0 (>12.5)	>250	17.2 (>14.5)	>250	>250
3	>250	>250	>250	23.0 (>10.9)	>250	7.8 (>32.0)	>250	>250
4	>250	>250	>250	160.7 (>1.5)	>250	56.9 (>4.4)	>250	>250
5	>250	>250	>250	71.8 (>3.5)	>250	>250	>250	>250
6	>250	>250	>250	>250	>250	>250	>250	>250
7	181.8 (0.5)	48.9 (2.0)	38.7 (2.5)	62.1 (1.5)	94.7 (1.0)	14.4 (6.7)	111.0 (0.9)	95.9
8	>250	>250	>250	>250	>250	>250	>250	>250
9	>250	>250	>250	74.7 (>3.3)	>250	>250	>250	>250
10	>250	39.4 (>6.3)	>250	14.2 (>17.6)	>250	25.0 (>10.0)	83.5 (>3.0)	>250
11	>250	>250	194.8 (>1.3)	241.9 (>1.0)	>250	>250	>250	>250
12	>250	>250	>250	>250	>250	>250	>250	>250
13	>250	189.8 (>1.3)	48.7 (>5.1)	>250	>250	39.0 (>6.4)	69.1 (>3.6)	>250
14	>250	>250	>250	>250	>250	>250	>250	>250
15	>250	>250	90.5 (>2.7)	166.8 (>1.5)	>250	>250	>250	>250
16	208.5 (0.3)	26.2 (2.4)	17.5 (3.6)	0.4 (156.0)	57.3 (1.9)	10.2 (6.1)	4.1 (15.2)	62.4
17	193.8 (0.1)	>250	>250	12.1 (10.8)	207.2 (0.6)	>250	>250	130.8
18	>250	>250	>250	63.2 (>4.0)	>250	>250	>250	>250
19	>250	71.5 (>3.5)	>250	46.9 (>5.3)	>250	134.2 (>1.9)	106.2 (>2.3)	>250
20	>250	>250	>250	>250	>250	>250	>250	>250
21	96.7 (0.4)	45.5 (0.8)	71.7 (0.5)	82.5 (0.5)	112.6 (0.3)	16.0 (0.4)	188.3 (0.2)	38.6
22	58.2 (1.1)	67.6 (0.9)	19.8 (3.1)	54.4 (1.1)	26.3 (2.3)	10.6 (5.8)	90.0 (0.7)	62.0
23	>250	>250	>250	>250	>250	>250	>250	>250
24	>250	146.0 (>1.7)	>250	>250	>250	45.5 (>5.5)	>250	>250
25	>250	>250	23.3 (>10.9)	>250	>250	6.4 (>39.1)	>250	>250
DOX[b]	0.03 (1.0)	0.07 (0.4)	0.3 (0.1)	0.03 (1.0)	0.01 (3.0)	0.1 (0.3)	0.2 (0.1)	0.03

[a] GI_{50} is the concentration of compound ($\mu g \cdot mL^{-1}$) that inhibits cancer cell growth by 50%.
[b] Selectivity index was determined as the ratio of the GI_{50} value for HaCat to the GI_{50} value obtained for the cancer cell line.
[c] DOX is the reference drug doxorubicin.
[d] U251, glioma cells; MCF7, breast cancer cells; NCI/ADR-RES, multiple drug-resistant ovarian cancer cells; 786-0, renal cancer cells; NCI-H460, non-small lung cancer cells; PC-3, prostate cancer cells; HT29, colon cancer cells; HaCat, human keratinocyte cells.

3, **2**, and **10** also showed high degree of selectivity (≥10.0) for the PC-3 prostate cancer cells (Table 1). In fact, Ogbole et al. [30] classifies as non-cytotoxic compounds any substance that its SI values is higher than 20, while those which presents SI ≥ 10 is considered as a weak cytotoxic compound. Interestingly, some of these piperidine derivatives were also the most active as ROS scavengers (Fig. 4). Reactive oxygen species and the coupled oxidative stress have been associated with tumor formation [31]. Previous studies show that PC-3 prostate cancer cells generate high levels of ROS and inherent oxidative stress present in these cells is, in part, responsible for their proliferation and survival [31]. Thus, the neutralization of reactive oxygen species by these compounds can be directly related to their antiproliferative activities against PC-3 cells.

Compounds **2**, **3**, **10**, **16**, and **17** were also promising against 786-0 cells by exhibiting GI_{50} values lower than 25 $\mu g \cdot mL^{-1}$ and SI values higher than 10.0. Piperidine derivative **16**, with GI_{50} of 0.4 $\mu g \cdot mL^{-1}$, was the most active of series for this cell line (Table 1). The SI of **16** was 156.0, which means that this derivative is much more active against this renal cell line (786-0 cells) than to keratinocyte cells (HaCaT cells). Compared to other cancers, chemotherapy is rather ineffective for renal cell carcinoma. Many anticancer agents have been tested against renal cell carcinoma with most showing response rates of less than 10% [32–34]. Additionally to these lower efficacies, the toxicity profiles of the lead compounds to treat renal cell carcinoma seems to still be problematic issue that make a chemotherapy *per si* inefficient approach [35]. Taken all the above consideration, our results shows that piperidine derivative **16** is a lead compound for further studies in the *in vivo* models.

In general, U251, MCF7, NCI/ADR-RES, NCI-H460 and HT29 cells were least sensitive to the tested compounds. The most active compound against U251 cells was the derivative **22** (GI_{50} of 58.2 $\mu g \cdot mL^{-1}$) (Table 1). NCI/ADR-RES was resistant to most piperidine derivatives, except for compounds **16**, **22** and **25**, which showed GI_{50} values of 17.5, 19.8, and 23.3 $\mu g \cdot mL^{-1}$, respectively (Table 1). Compound **22** was also active against NCI-H460 cells (GI_{50} of 26.3 $\mu g \cdot mL^{-1}$) (Table 1). Finally, compound **16** was the most active against MCF7 (GI_{50} of 26.2 $\mu g \cdot mL^{-1}$) and HT29 (GI_{50} of 4.1 $\mu g \cdot mL^{-1}$) (Table 1). Interestingly, all compounds were considerably more toxic to the studied cancer cell lines than to the normal cell line HaCaT and the SI values of piperidine derivatives are, in general, higher than those presented by doxorubicin (DOX), a reference anticancer used in our studies (Table 1).

DNA-piperidines interaction studies

Interaction of piperidine derivatives with ctDNA by molecular fluorescence

The interaction between piperidine derivatives and ctDNA was evaluated by spectrofluorimetry technique, because it presents characteristics such as rapidity, high sensitivity, and provides information on the binding mode of the ligand in the macromolecule [36,37]. Therefore, the piperidine derivatives **7**, **8**, **9**, **10**, **16**, **21**, **22**, and **25** were selected, which present varied activity (low to high) against different human tumor cell lines. The compound **8** presented $GI_{50} > 250$ $\mu g \cdot mL^{-1}$ for all the cell lines evaluated and was considered the negative control. The piperidine **16** was considered the most active and selective compound, especially for 786-0 (renal cancer cells) with $GI_{50} = 0.4$ $\mu g \cdot mL^{-1}$ and selectivity index of 156.0. This way the compound **16** was used as the model for the presentation of the results.

The evaluated compounds have intrinsic fluorescence, thus were titrated with the ctDNA maintaining the concentration of the ligand fixed and varying the concentration of the macromolecule. In this assay, the compounds showed maximum

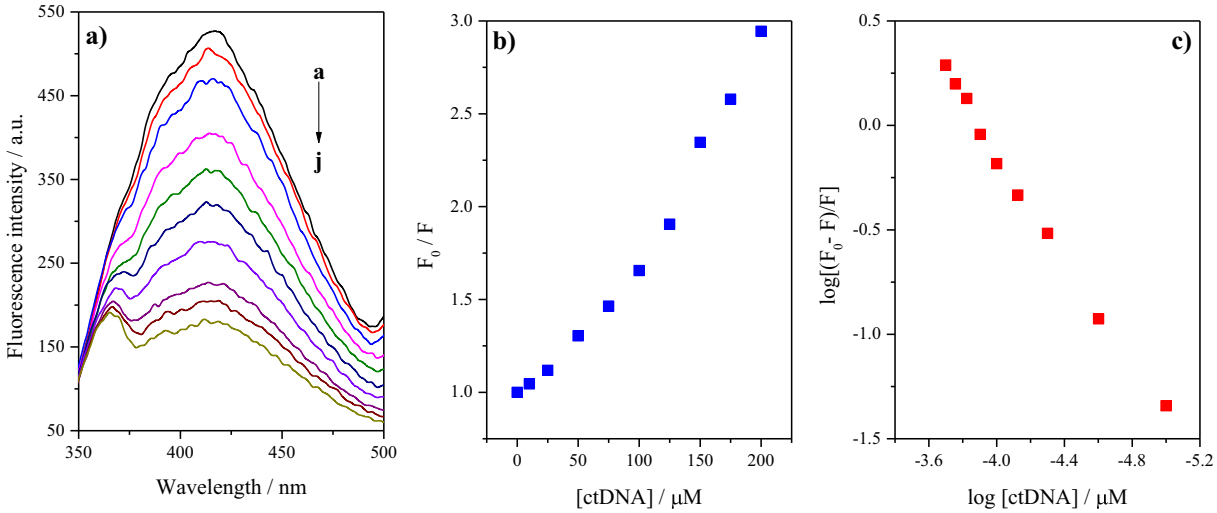

Fig. 5. Interaction of derivative **16** with ctDNA using fluorescence spectroscopy. (a) Fluorescence spectral profile of compound **16** (10 μM) in the presence of increasing concentrations of ctDNA: 0, 10, 25, 50, 75, 100, 125, 150, 175, and 200 μM, curves **a**-**j**, respectively). (b) Stern-Volmer plot for the quenching process at 25 °C. (c) Double logarithmic curve of DNA for interaction process compound **16** at 25 °C.

emission in the range from 350 to 442 nm, when excited between 246 and 278 nm, decreasing the analytical signal by increasing amounts of ctDNA to the system (Fig. 5a). The spectral changes represent a strong indication of that interaction process between the ctDNA and the evaluated ligands [38]. According to Mukherjee and Sing [39], this phenomenon is called quenching, and can occur by different mechanisms, generally classified by dynamic quenching, which occurs when the fluorophores (piperidines) in the excited state (F*) are deactivated upon contact with a quencher molecule (Q = ctDNA) during the existence of the excited state. Static quenching refers to the formation of a non-fluorescent supramolecular complex (F-Q) in the ground state, being independent of diffusion processes or molecular collisions [40]. The equation that describing this process is represented below:

$$\frac{F_0}{F} = 1 + K_q\tau_0[Q] \text{ or } \frac{F_0}{F} = 1 + K_{SV}[Q] \quad (1)$$

where $\mathbf{F_0}$ and $\mathbf{F}$ represent the fluorescence intensities in the absence and presence of the piperidine derivative, respectively; $\mathbf{K_q}$ is the diffusional bimolecular quenching rate constant (2.0×10^{10} L·mol^{-1}·s^{-1}), $\boldsymbol{\tau_0}$ is the average life time, typically 10^{-8} s, [36,41] **[Q]** is the concentration of the quencher, in this case the ctDNA and $\mathbf{K_{SV}}$ is the Stern-Volmer constant, calculated by the linearization of Eq. (1) (Fig. 5b). The interaction constant (K_b), to analyze the strength of the ctDNA-ligand binding was calculated, beyond of the parameter *n*, related to the number of binding sites in macromolecule (Fig. 5c) according to the equation below [42]:

$$\log\left(\frac{F_0 - F}{F}\right) = \log K_b + n\log[Q] \quad (2)$$

The values of the binding constant and number of sites are obtained through the slope and intercept of the logarithmic curve log[(F_0 − F)/F] *vs* log [ctDNA].

Additionally, from the K_b value, the thermodynamic parameter relative to free Gibbs energy (ΔG) was calculated to evaluate the spontaneity of the interaction process through the Eq. (3) described below [43]:

$$\Delta G = -RT\ln(K_b) \quad (3)$$

where T represents the temperature in Kelvin (K) and R is the ideal gas constant. Table 2 shows the results obtained for this evaluation.

The K_{SV} values ranged from 4.29 to 21.9×10^3 M^{-1}, indicating the signal decreasing in the presence of the quencher molecule (Table 2). In order to characterize the dominant quenching mechanism in the interaction process, the parameter K_q was evaluated. According to Dehkhodaei et al. [41] when this velocity constant is less than 2.0×10^{10} M^{-1} s^{-1}, the preferential quenching mechanism will be dynamic, whereas for higher K_q values it is indicative of static quenching. The K_q values ranged from 4.29 to 21.9×10^{11} M^{-1} s^{-1}, being higher than the limiting diffusional constant. Thus, static quenching is the dominant mechanism, characterized by the formation of supramolecular complex non-fluorescent in the ground state.

The K_b values ranged from 0.10 to 8.0×10^4 M^{-1} (Table 2), demonstrating the magnitude of the ctDNA-ligand interaction, which for most ligands is considered to be of medium affinity, except for compound **21** which showed constant in the order of 10^2, being classified as having low affinity [22]. Therefore, the values of binding constants with ctDNA followed the order: **16** > **22** > **10** > **25** > **9** > **7** > **8** > **21**, being the most active and selective compound (**16**), which showed the highest K_b value and consequently, the less active ones (**8** and **21**) showed the lowest values of binding constants.

The results obtained are in agreement with literature works, which evaluated the interaction of different compounds with the piperidine nucleus and DNA, such as: morphine ($K_b = 0.39 \times 10^4$ M^{-1}) [44], vincristine ($K_b = 1.70 \times 10^4$ M^{-1}) [45], vinblastine ($K_b = 0.17 \times 10^4$ M^{-1}) [46] and berberine ($K_b = 1.55 \times 10^4$ M^{-1}) [47]. Additionally, the preferred mode of binding for all compounds was by intercalation. Finally, the values of *n* were close to unity, showing a 1:1 stoichiometric ratio (DNA:ligand), and the ΔG values were all negative, characterizing the interaction process as spontaneous [48].

UV–visible spectroscopy studies

The UV–visible spectroscopy is a simple technique and has efficacy for detecting the formation of complexes between different ligands and macromolecules [36]. Thus, the Fig. S1 (Supplementary materials) shows the absorption spectrum of compound **16** in the absence and presence of DNA, and the free DNA.

The Fig. S1 shows that when ctDNA is added to the system, occurs an increase in absorbance (hyperchromic effect), indicating that there is interaction between the ligand and the biomolecule, with possible complex formation [49].

To confirm the existence of this interaction, it was made a spectrum of the difference between the ctDNA-piperidine complex and

Table 2
Interaction parameters of calf thymus DNA (ctDNA) with piperidines derivatives at 25 °C.

Compounds	Stern-Volmer constant			Binding parametrs			Thermodynamic parameter
	K_{sv} ($\times 10^3$ M^{-1})	r	K_q ($\times 10^{11}$ M^{-1} s^{-1})	K_b ($\times 10^4$ M^{-1})	*n*	r	ΔG (kJ mol^{-1})
7	5.80 ± 0.17	0.9959	5.80	1.67 ± 0.01	1.12 ± 0.04	0.9960	−24.1
8	4.29 ± 0.29	0.9862	4.29	0.92 ± 0.01	1.10 ± 0.01	0.9760	−22.6
9	10.4 ± 0.5	0.9897	10.4	2.19 ± 0.01	1.09 ± 0.06	0.9916	−24.8
10	8.98 ± 0.30	0.9954	8.98	4.26 ± 0.01	1.19 ± 0.02	0.9989	−26.4
16	9.58 ± 0.59	0.9852	9.58	8.00 ± 0.01	1.26 ± 0.04	0.9972	−27.9
21	6.08 ± 0.32	0.9917	6.08	0.10 ± 0.01	0.70 ± 0.02	0.9968	−6.47
22	21.9 ± 0.6	0.9978	21.9	6.02 ± 0.01	1.31 ± 0.04	0.9987	−27.3
25	9.68 ± 0.75	0.9796	9.68	2.88 ± 0.01	1.14 ± 0.09	0.9810	−25.4

the free ctDNA, verifying that the absorption spectra of the piperidine derivatives are not overlapping. These spectral changes are best observed from the absorbance values of the **16**-ctDNA mixture ($A_{complex}$ = 0.8626), and the sum of the absorbance values of the free compound and ctDNA ($A_{\mathbf{16}} + A_{ctDNA}$ = 0.5407). Through the equation $\Delta A = A_{complex} - (A_{compound} + A_{ctDNA})$, it is verified that the value of $\Delta A \neq 0$ (ΔA = 0.3219), which indicates that changes occurred in the fundamental state, characterizing a preferential mechanism of static quenching due to formation of a macromolecule-ligand complex [50], reinforcing the results by molecular fluorescence. However, if dynamic quenching was the predominant mechanism in the interaction process, one would not expect changes, since this affects only the excited state [22,51]. Similar behavior was observed for the other evaluated

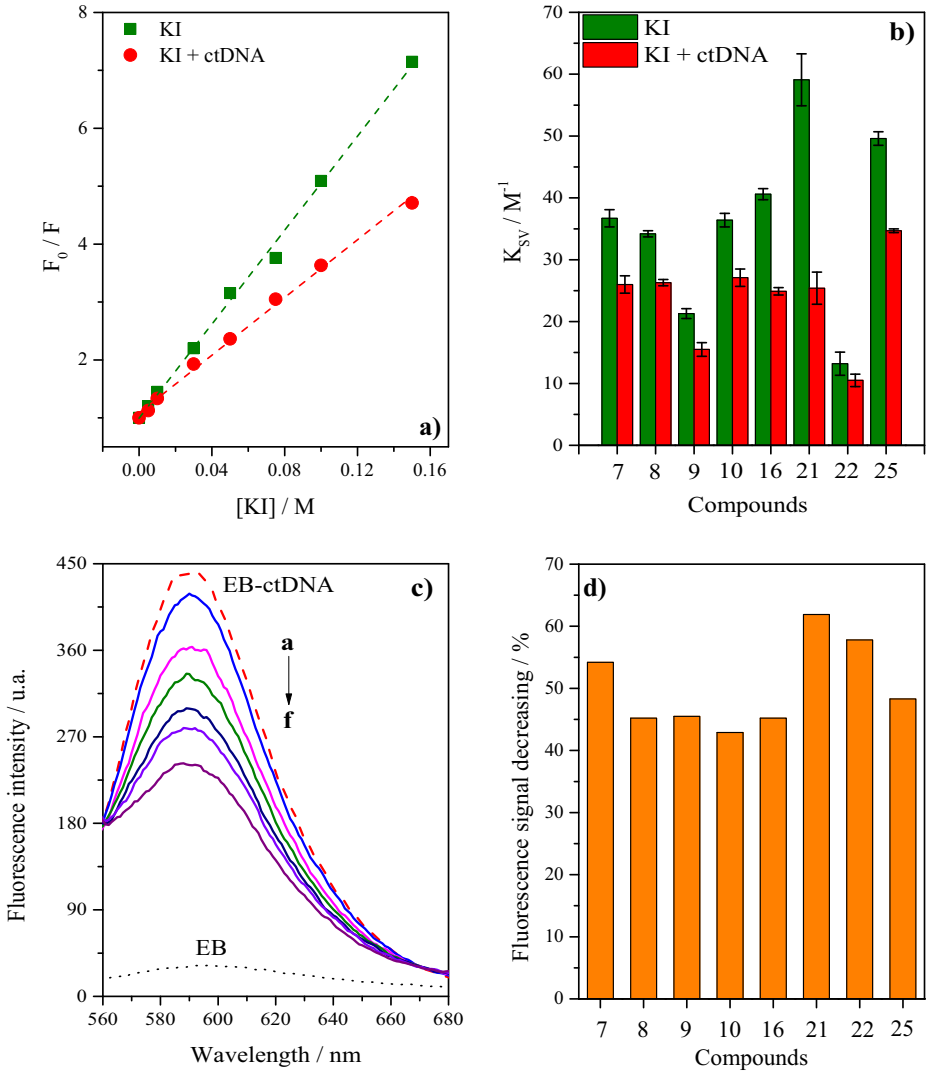

Fig. 6. Binding mode evaluation of ctDNA-ligand; (a) KI quenching assay. Stern-Volmer plot for fluorescence quenching of compound **16** by KI in the absence and presence of ctDNA (100 μM). (b) Stern-Volmer constant of piperidines derivatives (10 μM) quenching by KI in the absence and presence of ctDNA (100 μM). (c) Spectral profile of EB (2 μM) displacement in the ctDNA-EB complex by compound **16** in the concentration range of 10–60 μM, curves **a**-**f**, respectively. (d) Percentage of maximal decrease of ctDNA-EB complex signal in the presence of the piperidines derivatives.

piperidine compounds, as shown in Table S1 (Supplementary information).

Evaluation of the preferential DNA-ligand interaction mode

The binding mode of piperidine derivatives and ctDNA was evaluated from two assays: KI quenching study and competition with ethidium bromide. The results for this evaluation are summarized in Fig. 6.

KI quenching study

Fluorescence quenching studies provide information on the accessibility of the ligands to a fluorescence suppressor molecule, in this case the iodide ion [52]. This way, the magnitude of the Stern-Volmer constant in the presence and absence of ctDNA is evaluated, according to Eq. (1), where [Q] is equivalent to [KI]. Fig. 6a shows the fluorescence quenching of derivative **16** in the absence and presence of the macromolecule, and the K_{SV} values for all compounds evaluated are shown in Fig. 6b.

The K_{SV} values in the presence of ctDNA were systematically lower than in the absence of the macromolecule, indicating that the anion iodide failed to have access to the ligands (Fig. 6b), suggesting that they are protected by DNA base pairs, preventing the access of the anionic suppressor [53]. Thus, the main mode of binding these compounds to ctDNA occurs via intercalation.

Ethidium bromide (EB) competition assay

To confirm the results suggested by the KI assay, a competition study was performed with ethidium bromide, a classical probe that binds to DNA via intercalation. In aqueous solution, this competitor presents low fluorescence while free; however, when it binds to DNA the signal increases significantly due to its location between the nitrogenous base pairs [54]. Thus, any small molecule that replaces EB in the macromolecule will interact with the same binding mode [55]. In this sense, Fig. 6c shows that by adding increasing amounts of compound **16** to the system, a gradual decrease in the fluorescence signal occurs, evidencing that the EB is being displaced from the ctDNA.

The percentage of signal decrease ranged from 42.9 to 61.9% (Fig. 6d), using up to 30 times excess of the ligands over the initial amount of ethidium bromide. Thus, suggesting that the evaluated compounds interact preferentially by intercalation [56], confirming the previous results. Finally, the confirmation of the binding mode by intercalation corroborates with works of the literature that evaluated the interaction of compounds containing the piperidine nucleus with DNA [44–47].

Correlation of K_b values with IC_{50}

In order to infer the mechanism of action of the evaluated compounds, the correlation between the values of interaction constants (K_b) of the piperidines with ctDNA (Table 2) and the cytotoxic activity (GI_{50}) for the human cancer cell lines (Table 1) was stablished.

The correlation was performed only for the compounds with $GI_{50} < 250\ \mu g{\cdot}mL^{-1}$ values, which limited the number of points used in the mathematical modeling for each system. The compound **8** presented for all strains $GI_{50} > 250\ \mu g{\cdot}mL^{-1}$ (negative control), and thus was not used. The Fig. 7 shows the correlation coefficients obtained for the colon (HT-29), lung (NCI-H460), kidney (786-0) and resistant ovary lineages (NCI-ADR/RES), for the other lineages of tumor human cells and healthy cells, the correlation was not significant, where r < - 0.30.

According to Fig. 7, the compound that showed the highest interaction with ctDNA (piperidine derivative **16**), in general, was the most active against the cell lineages evaluated; while the less active compounds (piperidine derivatives **8** and **21**) were those

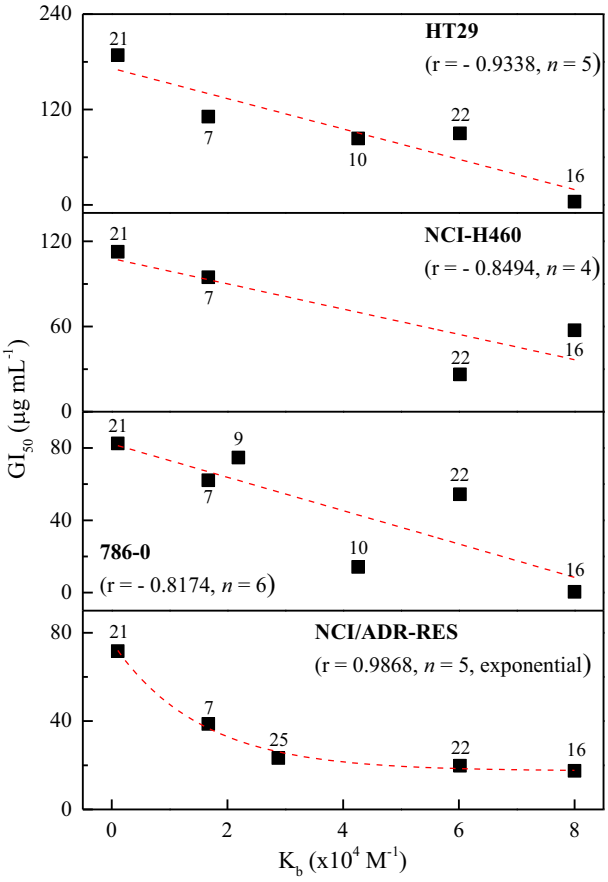

Fig. 7. Correlation between biological activity and DNA binding affinity of piperidines.

with the lowest ctDNA interaction constants. The values of the correlation coefficients obtained by the graph GI_{50} *vs* K_b showed correlation coefficient in the range of $0.8174 \leq |r| \leq 0.9868$, with the HT29, NCI-H460 and 786-0 lineages presenting a linear inverse tendency, while for NCI/ADR-RES was observed an inverse exponential relation. For these lineages, the GI_{50} value was inversely proportional to K_b, indicating that the interaction with DNA may be one of the possible mechanisms of action of these compounds.

The results are in agreement with same works in the literature that evaluated the correlation between interaction with DNA (K_b) and values of biological activity. Silva et al. [24] obtained a linear relation from $\log K_b$ between ctDNA and β-carboline derivatives with IC_{50} values (μM) for six human tumor cell lineages, with determination coefficients (r^2) from 0.5360 to 0.9600. In a similar evaluation, da Silva et al. [57] observed a linear relation from $\log K_b$ between ctDNA and Schiff bases with GI_{50} values ($\mu g{\cdot}mL^{-1}$) for seven human tumor cell lines, with correlation coefficients (r) from −0.9778 to +0.8693. Mckeever et al. [58] evaluated the interaction of DNA and antiprotozoal activity to guanidine diaromatic derivatives with $r^2 = 0.87$. Finally, Silva et al. [59] observed an exponential correlation between K_b and IC_{50} values (μM) for copper(II) ternary compounds with *N*-donor heterocyclic ligands and cytotoxic activity against chronic myeloid leukemia.

Molecular dynamics

Molecular dynamics associated with molecular docking studies have been successfully utilized in recognition of

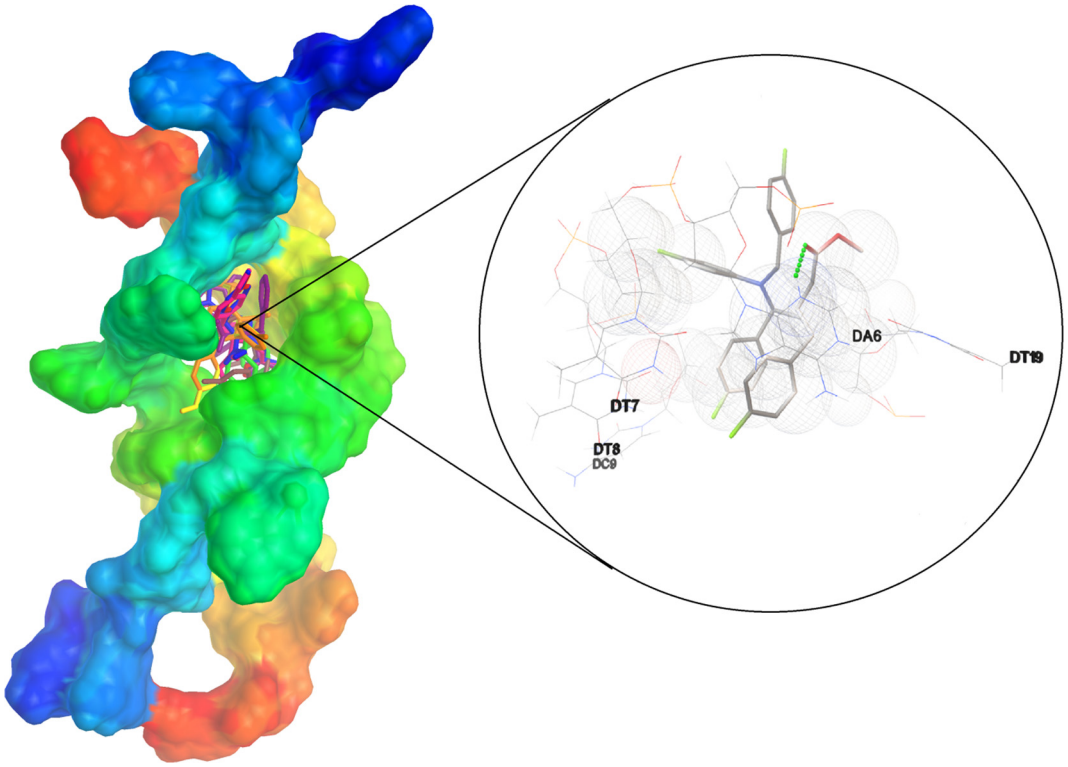

Fig. 8. Molecular docking poses (clustering) of the piperidine compounds in DNA generated by MD simulations. Schematic representation of compound **16**, which binds via intercalation. Green dots: H-bond; spheres: hydrophobic interactions.

Table 3
Comparative docking score, hydrophobic and H-bond interactions for each compound in this study.

Compound	Interactions		Docking score (kcal mol^{-1})
	Hydrophobic	H-bond (Å)	
7	DA6, DC9, DG16, DA17, DT19	–	−7.5
8	DG4, DA6, DC9, DA17, DT19	–	−7.6
9	DA6, DT7, DC9, DG10, DC11, DG16(π-π), DA18	DT8 with carbonyl (1.98)	−7.8
10	DA6, DT7, DC9, DG10, DC11, DG16(π-π), DT19	DT8 with carbonyl (2.04)	−7.5
16	DT7, DT8, DC9, DT19	DA6 with carbonyl (1.78)	−7.5
21	DA6, DC9(π-π), DG16(π-π), DA17(π-π), DT19(π-π)	–	−7.4
22	DC9, DG16, DA17, DT19	–	−7.1
25	DA6, DT8, DC9, DG16, DA17, DT19	–	−7.8

ligand-macromolecule interactions [60]. Dynamics simulation was performed to provide the native structure of the DNA in a physiological medium, after 6 ns. It was verified that the X-ray crystal DNA has a contracted conformation, which does not allow the ligands adopt intercalation binding mode into the macromolecule. Based on this, the molecular dynamics should be performed to allow a reorganization of the DNA bases, improving the spacing between them [61]. The molecular docking was performed to validate the binding mode of piperidine derivatives. Fig. 8 shows that the docked compounds bind the DNA via intercalation, and the complexes were stabilized mostly by π-π and hydrophobic interactions. The Figs. S2–S8 (supplementary information) present the results of theoretical studies for the other assessed piperidines derivatives.

Additionally, only the derivatives **9**, **10**, and **16** showed H-bond interactions involving carbonyl group (Table 3). Docking scores ranged of −7.1 to −7.8 kcal mol^{-1}, which corroborates high affinity towards DNA and are comparables with fluorescence spectroscopy results.

Conclusions

In conclusion, a series of twenty-five piperidines derivatives was evaluated as potential ROS and RNS scavengers and anticancer agents. Our results demonstrate that the evaluated piperidines possesses different abilities to scavenge the radical 2,2-diphenyl-1-picrylhydrazyl (DPPH) and the anion radical superoxide ($^{\cdot}O_2^-$). The piperidine **9** was the most potent radical DPPD scavenger (captured 44% of this radical when used at 64 μmol·L^{-1}), while the most effective to $^{\cdot}O_2^-$ scavenger was piperidine **10** (captured 42% of $^{\cdot}O_2^-$ when used at 80 μmol·L^{-1}). The behavior of the evaluated piperidines was also different against the human cancer cell lines studied. In general, U251, MCF7, NCI/ADR-RES, NCI-H460 and HT29 cells were least sensitive to the tested compounds and all compounds were considerably more toxic to the studied cancer cell lines than to the normal cell line HaCaT. In the ctDNA interaction studies was verified that the evaluated piperidine derivatives interact with the DNA model lead to formation of supramolecular complex, where K_b values ranged from 0.10 to 8.00 10^4 M^{-1}. In addition, by

correlating the binding constants with the GI_{50} values, it was observed that the correlation coefficients varied in the range of $0.8174 \leq |r| \leq 0.9868$, for HT29, NCI-H460, 786-0 and NCI/ADR-RES, suggesting that the preferential mechanism of action of these compounds may be associated with DNA as a biological target. The KI assay, competition with ethidium bromide and theoretical studies have suggested that such piperidine derivatives interact with DNA preferentially via intercalation. Finally, the docking and molecular dynamic studies confirmed the spectroscopic results obtained.

Conflict of interest

The authors have declared no conflict of interest.

Compliance with Ethics Requirements

This article does not contain any studies with human or animal subjects.

Appendix A. Supplementary material

Supplementary data associated with this article can be found, in the online version, at https://doi.org/10.1016/j.jare.2017.10.010.

References

[1] Behenna DC, Liu Y, Yurino T, Kim J, White DE, Virgil SC, et al. Enantioselective construction of quaternary *N*-heterocycles by palladium-catalyzed decarboxylative allylic alkylation of lactams. Nat Chem 2012;4(2):130–3.

[2] Patil PO, Bari SB. Nitrogen heterocycles as potential monoamine oxidase inhibitors: synthetic aspects. Arab J Chem 2014;7:857–84.

[3] Petit S, Nallet JP, Guillard M, Dreux J, Chermat R, Poncelet M, et al. Synthèses et activités psychotropes de 3,4-diarylpipéridines. Corrélation structure-activité et recherche d'une activité antihypertensive. Eur J Med Chem 1991;26:19–32.

[4] Zhou Y, Gregor VE, Ayida BK, Winters GC, Sun Z, Murphy D, et al. Synthesis and SAR of 3,5-diamino-piperidine derivatives: novel antibacterial translation inhibitors as aminoglycoside mimetics. Bioorg Med Chem Lett 2007;17:1206–10.

[5] Misra M, Pandey SK, Pandey VP, Pandey J, Tripathi R, Tripathi RP. Organocatalyzed highly atom economic one pot synthesis of tetrahydropyridines as antimalarials. Bioorg Med Chem 2009;17:625–33.

[6] Ho B, Crider AM, Stables JP. Synthesis and structure–activity relationships of potential anticonvulsants based on 2-piperidinecarboxylic acid and related pharmacophores. Eur J Med Chem 2001;36:265–86.

[7] Rao KN, Redda KK, Onayemi FY, Melles H, Choi J. Synthesis of some *N*-[pyridyl (phenyl)carbonylamino]hydroxyalkyl-(benzyl)-1,2,3,6-tetrahydropyridines as potential anti-inflammatory agents. J Heterocycl Chem 1995;32:307–15.

[8] Gangapuram M, Redda KK. Synthesis of 1-(substituted phenylcarbonyl/sulfonylamino)-1,2,3,6-tetrahydropyridine-5-carboxylic acid diethylamides as potential anti-inflammatory agents. J Heterocycl Chem 2006;43:709–18.

[9] Ravindernath A, Reddy MS. Synthesis and evaluation of anti-inflammatory, antioxidant and antimicrobial activities of densely functionalized novel benzo [*d*] imidazolyl tetrahydropyridine carboxylates. Arab J Chem 2017;10: S1172–9.

[10] Aeluri R, Alla M, Bommena VR, Murthy R, Jain N. Synthesis and antiproliferative activity of polysubstituted tetrahydropyridine and piperidin-4-one-3-carboxylate derivatives. Asian J Org Chem 2012;1:71–9.

[11] Wilkinson DG. The pharmacology of donepezil: a new treatment for Alzheimer's disease. Expert Opin Pharmacother 1999;1(1):121–35.

[12] Schotte A, Janssen PFM, Gommeren W, Luyten WHML, Van Gompel P, Lesage AS, et al. Risperidone compared with new and reference antipsychotic drugs: *in vitro* and *in vivo* receptor binding. Psychopharmacology 1996;124:57–73.

[13] Kosjek T, Dolinšek T, Gramec D, Heath E, Strojan P, Serša G, et al. Determination of vinblastine in tumour tissue with liquid chromatography–high resolution mass spectrometry. Talanta 2013;116:887–93.

[14] Brahmachari G, Das S. Bismuth nitrate-catalyzed multicomponent reaction for efficient and one-pot synthesis of densely functionalized piperidine scaffolds at room temperature. Tetrahedron Lett 2012;53:1479–84.

[15] Gülçin I. Antioxidant properties of resveratrol: a structure-activity insight. Innovat Food Sci Emerg Tech 2010;11:210–8.

[16] da Silva DL, Reis FS, Muniz DR, Ruiz ALTG, de Carvalho JE, Sabino AA, et al. Free radical scavenging and antiproliferative properties of Biginelli adducts. Bioorg Med Chem 2012;20:2645–50.

[17] Euzébio FPG, dos Santos FJL, Piló-Veloso D, Alcântara AFC, Ruiz ALTG, de Carvalho JE, et al. Synthesis, antiproliferative activity in cancer cells and theoretical studies of novel 6α,7β-dihydroxyvouacapan-17β-oic acid Mannich base derivatives. Bioorg Med Chem 2010;18:8172–7.

[18] Euzébio FPG, dos Santos FJL, Piló-Veloso D, Ruiz ALTG, de Carvalho JE, Ferreira-Alves DL, et al. Effect of 6α,7β-dihydroxyvouacapan-17β-oic acid and its lactone derivatives on the growth of human cancer cells. Bioorg Chem 2009;37:96–100.

[19] Marquissolo C, de Fátima Â, Kohn LK, Ruiz ALTG, de Carvalho JE, Pilli RA. Asymmetric total synthesis and antiproliferative activity of goniothalamin oxide isomers. Bioorg Chem 2009;37:52–6.

[20] Monks A, Scudeiro D, Skehan P, Shoemaker R, Paull K, Vistica D, et al. Feasibility of a high-flux anticancer drug screen using a diverse panel of cultured human tumor cell lines. J Natl Cancer Inst 1991;83(11):757–66.

[21] Mukherjee A, Mondal S, Singh B. Spectroscopic, electrochemical and molecular docking study of the binding interaction of a small molecule 5H-naptho[2,1-f] [1,2] oxathieaphine 2,2-dioxide with calf thymus DNA. Int J Biol Macromol 2017;101:527–35.

[22] Silva MM, Nascimento EOO, Júnior EFS, Júnior JXA, Santana CC, Grillo LAM, et al. Interaction between bioactive compound 11a-N-tosyl-5-deoxi-pterocarpan (LQB-223) and Calf thymus DNA: spectroscopic approach, electrophoresis and theoretical studies. Int J Biol Macromol 2017;96: 223–33.

[23] Silva-Júnior EF, Silva EPS, França PHB, Silva JPN, Barreto EO, Silva EB, et al. Design, synthesis, molecular docking and biological evaluation of thiophen-2-iminothiazolidine derivatives for use against *Trypanosoma cruzi*. Bioorg Med Chem 2016;24:4228–40.

[24] Silva MM, Savariz FC, Silva-Júnior EF, de Aquino TM, Sarragiotto MH, Santos JCC, et al. Interaction of β-Carbolines with DNA: spectroscopic studies, correlation with biological activity and molecular docking. J Braz Chem Soc 2016;27(9):1558–68.

[25] Machlin LJ, Bendich A. Free radical tissue damage: protective role of antioxidant nutrients. FASEB J 1987;1:441–5.

[26] Halliwell B. Free radicals, antioxidants, and human disease: curiosity, cause, or consequence? Lancet 1994;344:721–4.

[27] Prashanth MK, Revanasiddappa HD, Rai KML, Veeresh B. Synthesis, characterization, antidepressant and antioxidant activity of novel piperamides bearing piperidine and piperazine analogues. Bioorg Med Chem Lett 2012;22:7065–70.

[28] Stone SC, Vasconcellos FA, Lenardão EJ, do Amaral RC, Jacob RG, Leivas Leite FP. Evaluation of potential use of *Cymbopogon* sp. essential oils, (*R*)-citronellal and *N*-citronellylamine in cancer chemotherapy. Int J Appl Res Nat Prod 2013;6 (4):11–5.

[29] Sufian AS, Ramasamy K, Ahmat N, Zakaria ZA, Yusof MIM. Isolation and identification of antibacterial and cytotoxic compounds from the leaves of *Muntingia calabura* L. J Ethnopharmacol 2013;146:198–204.

[30] Ogbole O, Adeniji J, Ajaiyeoba E, Kamdem R, Choudhary M. Anthraquinones and triterpenoids from Senna siamea (Fabaceae) Lam inhibit poliovirus activity. Afr J Microbiol Res 2014;8(31):2955–63.

[31] Kumar B, Koul S, Khandrika L, Meacham RB, Koul HK. Oxidative stress is inherent in prostate cancer cells and is required for aggressive phenotype. Can Res 2008;68(6):1777–85.

[32] Rini BI, Vogelzang NJ, Dumas MC, Wade JL, Taber DA, Stadler WM. Phase II trial of weekly intravenous gemcitabine with continuous infusion fluorouracil in patients with metastatic renal cell cancer. J Clin Oncol 2000;18(12): 2419–26.

[33] Lilleby W, Foosa SD. Chemotherapy in metastatic renal cell cancer. World J Urol 2005;23:175–9.

[34] Stadler WM, Halabi S, Rini B, Ernstoff MS, Davila E, Picus J, et al. A phase II study of gemcitabine and capecitabine in metastatic renal cancer. Cancer 2006;107:1273–9.

[35] Nelson EC, Evans CP, Lara Jr PN. Renal cell carcinoma: current status and emerging therapies. Cancer Treat Rev 2007;33:299–313.

[36] Afrin S, Rahman Y, Sarwar T, Husain MA, Ali A, Shamsuzzaman, et al. Molecular spectroscopic and thermodynamic studies on the interaction of anti-platelet drug ticlopidine with calf thymus DNA. Spectrochim Acta A Mol Biomol Spectrosc 2017;186:66–75.

[37] Sirajuddin M, Ali S, Badshah A. Drug-DNA interactions and their study by UV-Visible, fluorescence spectroscopies and cyclic voltametry. J Photochem Photobiol, B 2013;124:1–19.

[38] Li J, Li B, Wu Y, Shuang S, Dong C, Choi MMF. Luminescence and binding properties of two isoquinoline alkaloids chelerythrine and sanguinarine with ctDNA. Spectrochim Acta A Mol Biomol Spectrosc 2012;95:80–5.

[39] Mukherjee A, Singh B. Binding interaction of pharmaceutical drug captopril with calf thymus DNA: a multispectroscopic and molecular docking study. J Lumin 2017;190:319–27.

[40] Darabi F, Hadadzadeh H, Ebrahimi M, Khayamian T, Rudbari HA. The piroxicam complex of cobalt(II): synthesis in two different ionic liquids, structure, DNA- and BSA interaction and molecular modeling. Inorg Chim Acta 2014;409:379–89.

[41] Dehkhodaei M, Khorshidifard M, Rudbari HA, Sahihi M, Azimi G, Habibi N, et al. Synthesis, characterization, crystal structure and DNA, HSA-binding studies of four Schiff base complexes derived from salicylaldehyde and isopropylamine. Inorg Chim Acta 2017;466:48–60.

[42] Movahedi E, Rezvani AR. New silver(I) complex with diazafluorene based ligand: synthesis, characterization, investigation of *in vitro* DNA binding and antimicrobial studies. J Mol Struct 2017;1139:407–17.
[43] Shujha S, Shah A, Zia-ur-Rehman Muhammad N, Ali S, Qureshi R, et al. Diorganotin(IV) derivatives of ONO tridentate Schiff base: synthesis, crystal structure, *in vitro* antimicrobial, anti-leishmanial and DNA binding studies. Eur J Med Chem 2010;45:2902–11.
[44] Li JF, Dong C. Study on the interaction of morphine chloride with deoxyribonucleic acid by fluorescence method. Spectrochim Acta A Mol Biomol Spectrosc 2009;71:1938–43.
[45] Mohammadgholi A, Rabbani-Chadegani A, Fallah S. Mechanism of the interaction of plant alkaloid vincristine with DNA and chromatin: spectroscopic study. DNA Cell Biol 2013;32(5):228–35.
[46] Tyagi G, Charak S, Mehrotra R. Binding of an indole alkaloid, vinblastine to double stranded DNA: a spectroscopic insight in to nature and strength of interaction. J Photochem Photobiol, B 2012;108:48–52.
[47] Li XL, Hu YJ, Wang H, Yu BQ, Yue HL. Molecular spectroscopy evidence of berberine binding to DNA: comparative binding and thermodynamic profile of intercalation. Biomacromol 2012;13:873–80.
[48] Zhang S, Sun X, Qu F, Kong R. Molecular spectroscopic studies on the interaction of ferulic acid with calf thymus DNA. Spectrochim Acta A Mol Biomol Spectrosc 2013;112:78–83.
[49] Sarwar T, Rehman SU, Husain MA, Ishqi HM, Tabish M. Interaction of coumarin with calf thymus DNA: deciphering the mode of binding by *in vitro* studies. Int J Biol Macromol 2015;73:9–16.
[50] Dantas MDA, Tenório HA, Lopes TIB, Pereira HJV, Marsaioli AJ, Figueiredo IM, et al. Interactions of tetracyclines with ovalbumin, the main allergen protein from egg white: spectroscopic and electrophoretic studies. Int J Biol Macromol 2017;102:505–14.
[51] Wu M, Wu W, Gao X, Lin X, Xie Z. Synthesis of a novel fluorescent probe based on acridine skeleton used for sensitive determination of DNA. Talanta 2008;75:995–1001.
[52] Jalali F, Dorraji PS. Interaction of anthelmintic drug (thiabendazole) with DNA: spectroscopic and molecular modeling studies. Arab J Chem 2017;10: S3947–54.
[53] Kundu P, Chattopadhyay N. Interaction of a bioactive pyrazole derivative with calf thymus DNA: deciphering the mode of binding by multi-spectroscopic and molecular docking investigations. J Photochem Photobiol, B 2017;173:485–92.
[54] Usman A, Ahmad M. Binding of Bisphenol-F, a bisphenol analogue, to calf thymus DNA by multi-spectroscopic and molecular docking studies. Chemosphere 2017;18:536–43.
[55] Rehman SU, Sarwar T, Husain MA, Ishqi HM, Tabish M. Studying non-covalent drug-DNA interactions. Arch Biochem Biophys 2015;576:49–60.
[56] Savariz FC, Foglio MA, Ruiz ALTG, da Costa WF, Silva MM, Santos JCC, et al. Synthesis and antitumor activity of novel 1-substituted phenyl 3-(2-oxo-1,3,4-oxadiazol-5-yl) β-carbolines and their Mannich bases. Bioorg Med Chem 2014;22:6867–75.
[57] da Silva CM, Silva MM, Reis FS, Ruiz ALTG, de Carvalho JE, Santos JCC, et al. Studies on free radical scavenging, cancer cell antiproliferation, and calf thymus DNA interaction of Schiff bases. J Photochem Photobiol, B 2017;172:129–38.
[58] McKeever C, Kaiser M, Rozas I. Aminoalkyl derivatives of guanidine diaromatic minor groove binders with antiprotozoal activity. J Med Chem 2013;56:700–11.
[59] Silva PP, Guerra W, dos Santos GC, Fernandes NG, Silveira JN, Ferreira AMC, et al. Correlation between DNA interactions and cytotoxic activity of four new ternary compounds of copper(II) with N-donor heterocyclic ligands. J Inorg Biochem 2014;132:67–76.
[60] Ajloo D, Moghadam ME, Ghadimi K, Ghadamgahi M, Saboury AA, Divsalar A, et al. Synthesis, characterization, spectroscopy, cytotoxic activity and molecular dynamic study on the interaction of three palladium complexes of phenanthroline and glycine derivatives with calf thymus DNA. Inorg Chim Acta 2015;430:144–60.
[61] Ajloo D, Sangian M, Ghadamgahi M, Evinic M, Saboury AA. Effect of two imidazolium derivatives of ionic liquids on the structure and activity of adenosine deaminase. Int J Biol Macromol 2013;55:47–61.